MANUSCRIPT TITLE

Comparative genomic analysis of multidrug-resistant clinical isolates of *Mycobacterium abscessus* revealed worldwide horizontal plasmid transfer

AUTHORS

Kensuke Ohse[1], Atsushi Yoshida[2,3,4], Keisuke Kamada[3,5], Hironobu Kitazawa[6], Yusuke Ito[7], Takayo Shoji[8], Kenichiro Watanabe[9], Hiroshi Koganemaru[2], Ken Kikuchi[3] and Masashi Toyoda[1,*]

[1] Research Team for aging science (Vascular Medicine), Tokyo Metropolitan Institute for Geriatrics and Gerontology (TMIG), 35-2 Sakaechou, Itabashi-ku, Tokyo, 173-0015, Japan

[2] Department of Infectious Diseases, TMIG, 35-2 Sakaechou, Itabashi-ku, Tokyo, 173-0015, Japan

[3] Department of Infectious Diseases, Tokyo Women's Medical University, 8-1 Kawada-Cho, Shinjuku-ku, Tokyo, 162-8666, Japan

[4] Department of Genetic Diagnosis and Laboratory Medicine, Dokkyo Medical University, 880 Kitakobayashi, Mibu Shimotsuga, Tochigi, 321-0293, Japan

[5] Department of Mycobacterium Reference and Research, The Research Institute of Tuberculosis, Japan Anti-Tuberculosis Association, 3-1-24 Matsuyama, Kiyose-shi, Tokyo, 204-8533, Japan

[6] Department of Pediatrics, Nagoya University Graduate School of Medicine, 65 Tsurumai-cho, Showa-ku, Nagoya-shi, Aichi, 466-8550, Japan

[7] Department of Pediatric Infectious Diseases, Hyogo Prefectural Amagasaki General Medical Center, 2-17-77 Higashi-Naniwa-cho, Amagasaki, Hyogo, 660-8550, Japan

[8] Department of Infectious Diseases, Shizuoka Children's Hospital, 860 Urushiyama, Aoi-ku, Shizuoka-shi, Shizuoka, 420-8660, Japan

[9] Department of Hematology and Oncology, Shizuoka Children's Hospital, 860 Urushiyama, Aoi-ku, Shizuoka-shi, Shizuoka, 420-8660, Japan

* To whom correspondence should be addressed. Tel: +81-3-3964-3241; Fax: +81-3579-4776; Email: mtoyoda@tmig.or.jp

Present Address: Hironobu Kitazawa, Department of Hematology and Oncology, Children's Medical Center, Japanese Red Cross Aichi Medical Center Nagoya First Hospital, 3-35 Michishita-cho, Nakamura-ku, Nagoya, 453-8511, Japan

GRAPHICAL ABSTRACT

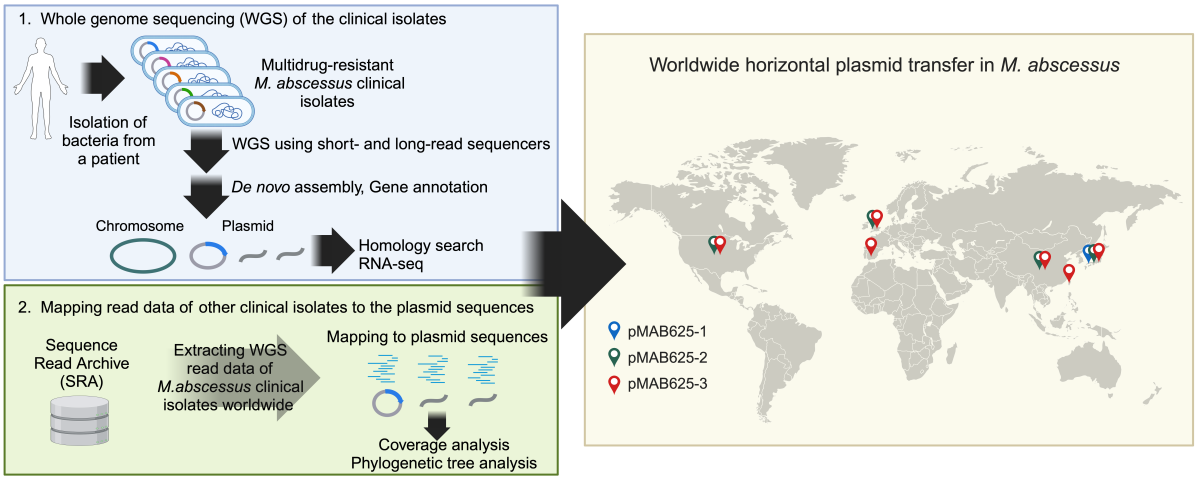

ABSTRACT

In recent years, the number of infections caused by non-tuberculous mycobacteria has increased worldwide, and infections caused by *Mycobacterium abscessus* (*M. abscessus*) are often difficult to treat due to their multidrug resistance. Research into the mechanisms of multidrug resistance in *M. abscessus* has focused on genetic mutations but not on genetic mobile elements such as plasmids. We performed a comparative genomic analysis of clinical isolates of *M. abscessus* collected from the same patient at different time points. Antimicrobial susceptibility testing showed that these clinical isolates had decreased susceptibility to carbapenem antibiotics compared to the type strain. Although the isolates had relatively few chromosomal mutations, they harboured three plasmids not found in the type strain. Two of the three plasmids encoded genes such as the ESX secretion system, and the other encoded the MMPL family transporter. We also mapped the sequence data from clinical isolates collected worldwide to these plasmid sequences. The data from 2.2% and 11.3% of isolates were mapped entirely to two of these plasmid sequences, respectively. These results indicate that these plasmids have been horizontally transferred among clinical isolates of *M. abscessus* worldwide and provide new insights into the acquisition of multidrug resistance in *M. abscessus*.

INTRODUCTION

In recent years, the global incidence of non-tuberculous mycobacterial infections has been on the rise, presenting a significant challenge due to their increasing prevalence and innate drug resistance, particularly in *M. abscessus* infections (1). *M. abscessus* is not limited to pulmonary infections but also serves as the causative agent for various extrapulmonary infections, including bloodstream, skin, soft tissue, surgical site, and peritoneal dialysis-related infections (2). Furthermore, it demonstrates resistance to a wide range of antimicrobial agents.

The resistance mechanism has been thoroughly investigated, primarily concerning macrolide antibiotics, which are regarded as essential drugs, and the involvement of the *erm* and *rrl* genes has been elucidated (3–5). The Clinical and Laboratory Standards Institute (CLSI) also recommends an analysis of the *erm* gene in microbiological laboratories (6). Among *M. abscessus* strains with a non-truncated *erm*(41) gene, the most common variant is T28 sequevar, which has been observed to exhibit inducible resistance to macrolides. However, it has been pointed that *M. abscessus* subsp. *abscessus* (ABS) can develop inducible resistance even without T28 (7), and that although whole genome sequences (WGS) are useful for predicting resistance, they are not sufficient (8, 9).

We conducted whole-genome sequencing of *M. abscessus* subsp. *massiliense* (MAS), which developed intravascular infections and subsequently became resistant to clarithromycin during treatment. Despite having a non-functional *erm* gene and no *rrl* mutation, we were unable to identify any mutations in the genome that could explain macrolide resistance in this strain with sufficient evidence (10). This highlights the existence of strains for which the mechanism of antimicrobial resistance remains unexplained by WGS.

Regarding other antimicrobial agents, apart from resistance genes for amikacin and fluoroquinolones, there is limited information available about the correlation between genomic variations and resistance, and such information is mostly confined to a few antimicrobial agents. Therefore, despite the comprehensive genomic data provided by WGS, identifying the genes responsible for resistance, especially in cases of multi-drug resistance, remains challenging. As a result, the utility of WGS in predicting resistance remains inconclusive.

In this study, we observed elevated minimum inhibitory concentrations (MICs) for carbapenem antibiotics in a case of disseminated infection caused by ABS T28 sequevar during

antimicrobial therapy. Several causes of the decreased susceptibility to carbapenem antibiotics have been reported, including the acquisition of the carbapenemase (11), efflux pump overexpression (12), and mutations in PBPs (13). However, the mechanism of the increased resistance to carbapenem antibiotics in *M. abscessus* was unclear. We then performed *de novo* genome assembly of the strains isolated sequentially from this patient, including chromosome as well as plasmid, by WGS using short- and long-read sequencers. We present the results, which suggest the involvement of plasmids in the mechanism of antimicrobial resistance. Taking these results, we re-analysed the read data obtained by WGS from clinical isolates of *M. abscessus* using a short-read sequencer deposited in the public database. We found that the data from 2.2% and 11.3% of isolates collected worldwide were mapped to the two plasmid sequences, suggesting that these plasmids have been horizontally transferred among clinical isolates of *M. abscessus* worldwide.

MATERIAL AND METHODS

Clinical isolates and type strain

Ethical approval for this study was obtained from the Ethics Committee of Dokkyo Medical University (approval number 28045). Regarding Isolate57625, Isolate57629, Isolate57630, Isolate57596, and Isolate57626, specimens were obtained from a patient with osteomyelitis at the five time points in six months indicated in Table 1. Each strain was isolated from the specimen at Shizuoka Children's Hospital for diagnosis. The other clinical isolates used for PCR or WGS were stored in TMIG or Tokyo Women's Medical University or Dokkyo Medical University (14). The type strain of ABS, ATCC 19977, was purchased from ATCC (VA, US). The type strain of MAS, JCM 15300, and the type strain of *M. abscessus* subsp. *bolletii* (BOL), JCM 15297, were provided by Japan Collection of Microorganisms, RIKEN BRC which is participating in the National BioResource Project of the MEXT, Japan.

Growth curve

The type strain and the five clinical isolates were inoculated onto trypticase soy agar (TSA) with 5% sheep blood (Beckton Dickinson, NJ, US) and incubated at 30 °C for five days. Next, some colonies were inoculated into BBL™ Mueller Hinton II Broth (Cation-Adjusted) (Beckton Dickinson) and incubated overnight at 30°C. These culture medium were measured for

absorbance (OD_{600}), from which they were prepared to 0.1 by medium. Seventy microliter of the adjusted culture solution was inoculated into 7 mL of BBL™ Mueller Hinton II Broth (Cation-Adjusted) and incubated at 30 °C for eight days with agitation (200 rpm). OD_{600} was measured on days one to eight after inoculation. Statistical analysis was performed using R ver. 4.3.1.

Antimicrobial susceptibility testing

The type strain and the clinical isolates were subcultured on 2% OGAWA medium (Kyokuto Pharmaceutical Industrial, Tokyo, Japan) at 30 °C for five days. Antimicrobial susceptibility testing was performed using BrothMIC RGM (Kyokuto Pharmaceutical Industrial) following CLSI M24 ED3rd (6). Minimum inhibitory concentrations (MICs) were determined as the minimum concentration at which bacteria had not grown on day four (all antibiotics) and day 14 (clarithromycin). The test was repeated three times and all MICs were confirmed to be the same between the experiments, except for imipenem (IPM) for the isolates. For IPM, the MICs of the type strain were confirmed to be the same between all three experiments, while for the MICs of Isolate57625 and Isolate57626 they were confirmed to be the same between two out of three experiments, as indicating in the Table 1.

Mycobacterial DNA isolation and whole-genome sequencing

The type strain and the clinical isolates of *M. abscessus* were stored in frozen stock containing skim milk and 5% (v/v) glycerol. Each strain was inoculated from frozen stocks into Middlebrook 7H9 Medium (Sigma-Aldrich, MO, US) containing 10% (v/v) oleic acid-albumin-dextrose-catalase (OADC) and 0.2% (v/v) glycerol and cultured at 30 °C for six days with agitation (200 rpm). Bacterial genomic DNA for short-read sequencing was extracted as previously reported (15). The quality of the extracted DNA was confirmed by agarose gel electrophoresis, and the concentration was measured using Qubit™ BR DNA Quantitation Kit (Thermo Fisher Scientific, MA, US). Genomic DNA was fragmented, and the sequencing library was prepared using the Ion Xpress™ Plus Fragment Library Kit and the Ion Xpress™ Barcode Adapters 1-96 kit (Thermo Fisher Scientific) according to the manufacturer's instructions. The quantity of sequencing library was assessed using the Ion Library TaqMan™ Quantitation Kit (Thermo Fisher Scientific). Emulsion PCR for sequence template synthesis was performed with the Ion PI™ Hi-Q™ OT2 200 Kit v2 using the Ion One Touch™ II System and the Ion One

Touch™ II ES (Thermo Fisher Scientific). Sequencing was performed using the Ion PI™ Chip kit v3 and the Ion Proton™ System (Thermo Fisher Scientific). Data were collected using the Torrent Suite v5.0.5 software (Thermo Fisher Scientific).

High-molecular-weight genomic DNA for long-read sequencing was extracted as follows. The bacterial pellet was collected by centrifugation and homogenised using EZ-beads (Promega, WI, US) and Shakeman 6 (Bio Medical Science, Tokyo, Japan). The homogenised pellet was lysed with Lysozyme (Sigma-Aldrich, L4919) at 37 °C for one hour. Next, DNA was extracted using Wizard® HMW DNA Extraction Kit (Promega) following the manufacturer's instructions. Fragmented DNA in the extracted DNA was removed using the Short Read Eliminator Kit (PacBio, CA, US). The sequencing library for long-read sequencing was prepared using the Ligation Sequencing Kit (SQK-LSK109, Oxford Nanopore Technologies, Oxford, UK) and the Native Barcoding Expansion 1-12 (EXP-NBD104, Oxford Nanopore Technologies). In brief, the barcode sequences for multiplex sequencing were attached to the ends of the HMW genomic DNA. In addition, the sequencing adapters were ligated to the end of HMW genomic DNA. The prepared DNA was loaded into a flow cell (FLO-MIN106, Oxford Nanopore Technologies) attached to MinION Mk1B (Oxford Nanopore Technologies). Sequencing data were acquired using MinKNOW ver.21.06.0 (Oxford Nanopore Technologies), and base calling was performed using Guppy ver. 5.0.7 (Oxford Nanopore Technologies) with high accuracy mode using the National Institute of Genomics supercomputer system (NIG, Shizuoka, Japan). Data quality was confirmed using NanoPlot ver. 1.38.0 (16) and adapter sequences were trimmed using Porechop ver. 0.2.4 (17). Raw reads shorter than 1000 bp (Isolate57625, Isolate57629, Isolate57630, Isolate57596) or 5000 bp (Isolate57626) were removed using Filtlong ver. 0.2.1 (https://github.com/rrwick/Filtlong). Filtered reads were corrected using Fmlrc ver. 1.0.0 (18) with the data of short-read sequencing acquired by the Ion Proton™ Sequencer. *De novo* assembly was performed using Flye ver. 2.9-b1768 (19) with corrected long-reads. Assembled genome sequences were polished using Pilon ver. 1.24.0 (20), evaluated using QUAST ver. 5.0.2 (21), and visualised using Bandage ver. 0.8.1 (22). Genome annotation was performed using DFAST v.1.5.0 (23, 24). Plasmid sequences were searched using the PLSDB website (25).

Single nucleotide variants and structural variants analysis

Short-read data acquired by the Ion Proton™ Sequencer were mapped using BWA-MEM ver. 0.7.17-r1188 (26) against the reference sequence (CU458896.1, CU458745.1). Output BAM files were sorted using samtools ver.1.12 (27). Valiant calling was performed using Freebayes ver. 1.3.5 (28), and variants were annotated using SnpEff ver. 5.2 (29) with annotated genome sequence. The positions of single nucleotide variants (SNVs) were visualised using IGV (Broad Institute, MA, US). Assembled genome sequences were aligned using Mauve ver. 2.4.0 (30) for structural variant (SV) analysis. Mapping the short- and long-read to the assembled genome sequence using minimap2 ver. 2.21-r1071 (31) was performed for the validation of assembly.

PCR for the validation of SVs was performed using KOD One® PCR Master Mix (TOYOBO, Osaka, Japan) and the primers indicated in Supplementary Table S1. Amplified DNA was confirmed using agarose gel electrophoresis following staining with SYBR™ Safe Gel Stain (Thermo Fisher Scientific).

Phylogenetic tree analysis

The genome sequences of the various clinical isolates shown in Figure 2C for phylogenetic tree analysis were obtained from the NCBI database and are listed in Supplementary Table S2. Core-genome SNVs were detected using Snippy ver. 4.6.0 (https://github.com/tseemann/snippy) with each assembled genome sequence and the type strain (ATCC 19977, CU458896.1) as the reference. The concatenated core-genome SNVs were also aligned using the snippy-core script. The phylogenetic tree was constructed using IQ-TREE ver.2 (32) using the maximum likelihood criterion and rendered using iTOL ver.6.7 (33). For the phylogenetic tree analysis regarding the components of the ESX secretion system, the amino acid sequences of ESX loci (*eccB*, *eccC*, *eccD*, *mycP*, and *eccE*) were concatenated and used as input for NGphylogeny.fr (34) using the PhyML+SMS inference method.

Homology search of antimicrobial resistance genes

Homology search was performed by blast+ (35) using the amino acid sequence as the query or by Abricate software (http://github.com/tseemann/abricate) using the nucleotide sequences as the query. NCBI AMRFinderPlus (36), CARD (37), Resfinder (38), ARG-ANNOT (39), VFDB (40), PlasmidFinder (41), EcOH (42), and MEGARes 2.00 (43) were used as the database for the search of antimicrobial resistance genes. Mycobrowser (44) was used as the database for the homology search of the mycobacterium genes.

PCR for plasmid detection and copy number analysis

PCR was performed using KOD One® PCR Master Mix (TOYOBO) and the primers indicated in Supplementary Table S1. Amplified DNA was confirmed using agarose gel electrophoresis. The plasmid copy number was analysed by qPCR using PowerUp™ SYBR™ Green Master Mix (Thero Fisher Scientific). qPCR was performed using the QuantStudio™ 5 Real-Time PCR System (Thermo Fisher Scientific). Five nanogram of genomic DNA was used for a 20 μL reaction volume of qPCR.

RNA-seq analysis

Total RNA was extracted as follows: The bacterial pellet was collected by centrifugation and suspended in UltraPure™ DNase/RNase-free Distilled Water (Thermo Fisher Scientific) and homogenised using EZ-beads (Promega) and Shakeman 6 (Bio Medical Science). SUPERase-In™ RNase Inhibitor (Thermo Fisher Scientific) was added to the homogenised pellet. Next, the homogenised pellet was lysed by Lysozyme (Sigma-Aldrich) at 37 °C for an hour. Total RNA was purified by mirVana™ miRNA Isolation Kit (Thermo Fisher Scientific). The size and quality of total RNA were assessed using the Agilent 2100 Bioanalyzer (Agilent Technologies, CA, US) and the RNA 6000 Nano Kit. rRNA was depleted using the NEBNext® rRNA Depletion Kit (Bacteria) (NEB, MA, US) from 500 ng of total RNA. The whole transcriptome library was prepared using the Ion Total RNA-Seq Kit v2 (Thermo Fisher Scientific) as follows: First, the rRNA-depleted RNA was fragmented by RNase III at 37 ˚C for 10 minutes and purified using the Magnetic Beads Cleanup Module. Next, adapter sequences were ligated and reverse transcription was performed. The whole transcriptome library was amplified and barcoded using the IonXpress™ RNA-Seq Barcode 1-16 Kit (Thermo Fisher Scientific). The quantity of the amplified whole transcriptome library was assessed using the Ion Library TaqMan™ Quantitation Kit (Thermo Fisher Scientific). Emulsion PCR for sequence template synthesis was performed using the Ion PI™ Hi-Q™ OT2 200 Kit v2 with the Ion One Touch™ II System and the Ion One Touch™ II ES (Thermo Fisher Scientific). Sequencing was performed using the Ion Proton™ System with Ion PI™ Chip kit v3 (Thermo Fisher Scientific). Data was collected using the Torrent Suite ver. 5.0.5 software (Thermo Fisher Scientific). Sequence reads were mapped using Bowtie ver. 1.0.0 (45) against the assembled genome sequence of Isolate57625. Mapped reads were counted using HTseq ver. 1.99.2 (46). Merged transcript count data were

normalized using TCC ver. 1.26.0 (47) and differentially expressed genes (DEG) were detected under false discovery rate (FDR) < 0.01.

Mapping the read data of various clinical isolates to the genome sequence of Isolate57625

Raw read data of *M. abscessus* clinical isolate in Japan, Taiwan (48), China (49), the US, the United Kingdom (UK) and Spain were obtained from the NCBI Sequence Reads Archive (SRA). Raw read data were trimmed using fastp ver. 0.23.4 (50) and reduced using seqkit ver.2.4.0 (51) to 200 Mb for the Ion Proton™ single-end data and 100 Mb for the Illumina pair-end data to equalise the depth of coverage among isolates. Reads were mapped using BWA-MEM ver. 0.7.17-r1188 against the chromosome and plasmid sequences of Isolate57625. The depth of coverage was calculated using Qualimap ver. 2.2.2-dev (52). We checked the mapping results using IGV regarding the isolates whose mean of coverage to the pMAB625 plasmids sequences was more than zero. We considered the isolates whose data were mapped to the almost the entire region of the pMAB625 sequences as the plasmid-harbouring isolates. For the phylogenetic tree analysis of the worldwide isolates, the data of ABS and MAS were used because no pMAB625 plasmid was detected in BOL. The full sequences aligned using Snippy-core script were used as input for Gubbins ver.3.3.1 (53). The phylogenetic tree was rendered using ggtree ver 3.10.1 (54).

RESULTS

Antimicrobial Susceptibility Testing of the clinical isolates

We first compared the growth rate of the type strain (ATCC 19977) and two isolates, Isolate57625 and Isolate57626. The growth rates of Isolate57625 and Isolate57626 were significantly slower than the type strain (Figure 1). To investigate the antimicrobial susceptibility of two clinical isolates, we next performed antimicrobial susceptibility testing using BrothMIC RGM, which can measure the MIC of various antibiotics according to CLSI M24 ED3rd. This analysis showed that the MIC of Isolate57626 against IPM, which binds the penicillin-binding proteins (PBPs) and inhibits the synthesis of the bacterial cell wall, was higher than that of the type strain, and the MICs of Isolate57625 and Isolate57626 against

meropenem (MEPM), which has the same mechanism of action as IPM and enhanced stability, were higher than that of the type strain (Table 1). However, there were no differences in MIC between ATCC 19977 and two isolates against the other antibiotics. These results indicated the decreased susceptibility of the isolates to carbapenem antibiotics compared to the type strain.

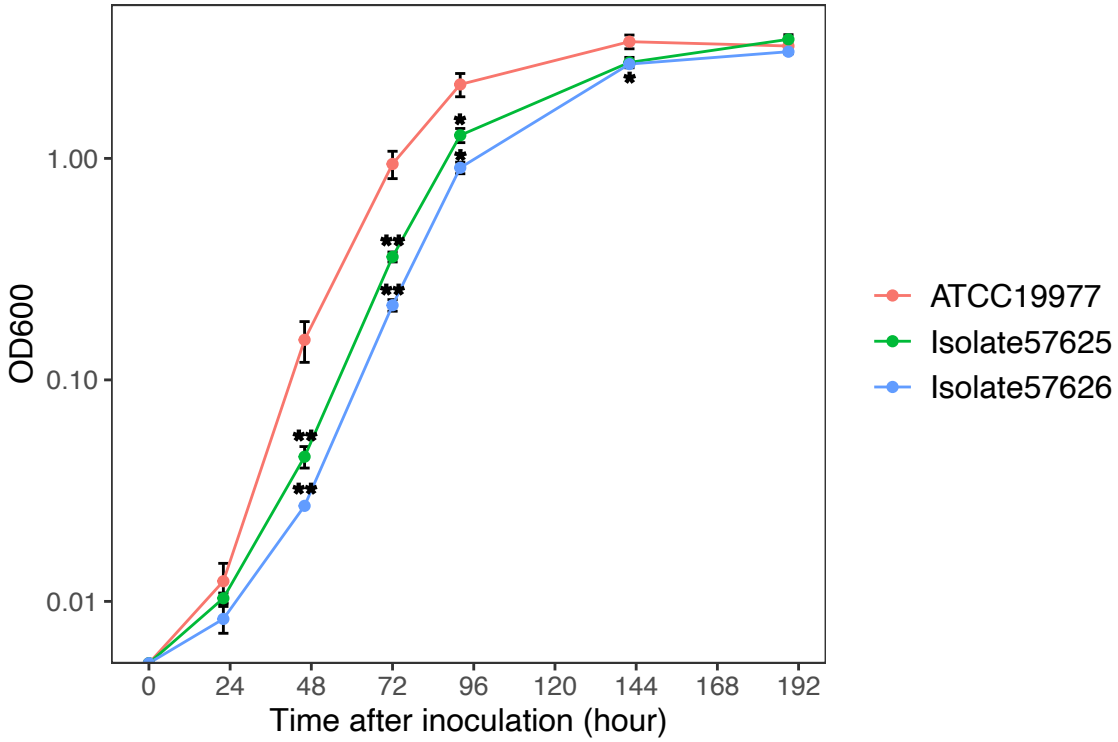

Figure 1. Growth curve of the type strain and the isolates. The type strain (ATCC 19977) and the isolates were inoculated with the same seeding concentration and cultivated at 30 °C. OD_{600} was measured at each time point. Data represents the mean of the three independent experiments and the error bar represents the standard deviation. Asterisks represent the statistical significance between ATCC 19977 and each isolate. *p*-value were calculated using one-way ANOVA followed by Dunnett's test (*$p<0.01$, **$p<0.001$).

Table 1. The isolation time point of the clinical isolates and antimicrobial susceptibility of the type strain and the isolates

Isolates	Source	Period from the first isolation (month)	MIC* (μg/mL)														
			AMK	TOB	IPM	FRPM	LVFX	MFLX	AZM	CAM 4day	CAM 14day	ST	DOXY	MEPM	LZD	CLF	STFX
ATCC 19977	-	-	8	8	16	>64	32	>8	64	2	>64	>152/8	>16	64	32	1	2
Isolate57625	catheter	0	8	8	16†	>64	16	>8	64	2	>64	>152/8	>16	>64	32	1	2
Isolate57629	catheter	4	-	-	-	-	-	-	-	-	-	-	-	-	-	-	-
Isolate57630	bone biopsy	4	-	-	-	-	-	-	-	-	-	-	-	-	-	-	-
Isolate57596	heel	6	-	-	-	-	-	-	-	-	-	-	-	-	-	-	-
Isolate57626	malleolus	6	8	8	>64‡	>64	32	>8	64	2	>64	>152/8	>16	>64	32	1	2

*MICs were determined as the minimum concentration at which the bacteria did not grow. No antimicrobial susceptibility testing was conducted on the isolates other than Isolate57625 and Isolate57626, representing hyphens in the table. The test was repeated three times and all MICs were confirmed to be the same between the experiments with exception of imipenem for the isolates. AMK, Amikacin; TOB, Tobramycin; IPM, Imipenem; FRPM, Faropenem; LVFX, Levofloxacin; MFLX, Moxifloxacin; AZM, Azithromycin; CAM, Clarithromycin; ST, Trimethoprim/sulfamethoxazole; DOXY, Doxycycline; MEPM, Meropenem; LNZ, Linezolid; CLF, Clofazimine; STFX, Sitafloxacin

†For Isolate57625, the MICs against IPM in the three experiments were 64, 16, and 16 μg/mL, respectively.

‡For Isolate57626, the MICs against IPM in the three experimenst were >64, 16, and >64 μg/mL, respectively.

Table 2. Genome assembly and the annotation statics of the Isolate57625

Contig	Form	Length(bp)	GC contents (%)	Number of CDS	Number of rRNA	Number of tRNA	Number of tmRNA
Chromosome	circular	5,072,346	64.1	5,034	3	48	1
pMAB625-1	linear	202,398	64.7	247	0	29	0
pMAB625-2	linear	142,689	62.2	171	0	0	0
pMAB625-3	circular	24,988	65.6	30	0	0	0

The clinical isolates had chromosomes genetically close to the type strain and three plasmids not found in the type strain

To explore the factors that determine the difference in antimicrobial resistance between the type strain and the clinical isolates, we performed WGS using short-read sequencer and Nanopore long-read sequencer. We corrected the long-read sequence data using the short-read sequence data and performed *de novo* genome assembly using the corrected long-read sequence data. Two circularised contigs (contig1, 5 Mbp; contig2, 25 Kbp) and two linearised contigs (contig3, 203 Kbp; contig4, 140 Kbp) were obtained from each of the five clinical isolates. Considering that the chromosome size of the type strain is 5 Mbp, we concluded that contig1 was the chromosome and that the others were plasmids. We therefore named these three plasmids, contig3, 4, and 2, as pMAB625-1, pMAB625-2, and pMAB625-3, respectively. The length, GC content, number of coding sequences (CDS), rRNA, tRNA, and tmRNA encoded on the chromosome or each plasmid are indicated in Table 2. The CRISPR sequence was not detected in the genome of the isolates.

We next compared the chromosome sequence of the type strain and Isolate57625. SV analysis showed that two large insertions (13 kbp and 8 kbp) and a deletion (16 kbp) existed in the assembled chromosome sequence of Isolate57625 (Figure 2A). We confirmed these insertions and deletion by PCR using the primes (Supplementary Table S1) that were designed for the regions flanking the insertions and the deletion site (Figure 2B). The coding sequences of phage integrase and transposase were present near the three large SVs (Supplementary Figure S1), indicating that these regions were prophage. Twenty genes were acquired and 25 genes were lost in Isolate57625 compared to the type strain by SVs in the chromosome (Supplementary Table S3). However, the proteins translated from these genes have not been reported to be associated with antimicrobial resistance. In addition, 34 missense mutations, and nine frameshift mutations were detected in the chromosome sequence of the clinical isolates (Supplementary Table S3). Because these mutations have not been reported as the cause of antimicrobial resistance, further functional analysis will be required to verify whether these variants affect antibiotic resistance. To analyse the difference in the chromosome sequence between the clinical isolates, we analysed SVs and SNVs between the isolates. This analysis revealed that a 6500 bp insertion, a 500 bp deletion, and six SNVs existed in the chromosome of Isolate57626, the most recently isolated strain, compared to the other strains

(Supplementary Figure S2). These six SNVs were missense mutations at different gene loci, and five of six mutations have not been reported as the cause of antibiotic resistance. However, one mutation was located at the putative *PbpA*, which was associated with the synthesis of the bacterial cell wall and the target of carbapenem antibiotics, suggesting that this SNV may be responsible for the reduced susceptibility of Isolate57626 to IPM compared to Isolate57625 (Supplementary Figure S2B, Table 1).

To investigate the genetic distance of chromosomes between Isolate57625 and other *M. abscessus* strains, we further performed phylogenetic tree analysis using the complete genome sequences deposited in the GenBank database (Figure 2C). This analysis revealed that Isolate57625 was genetically close to the type strain among ABS strains.

Taken together, given the genetic distance of the chromosome and the number of genes acquired by plasmid acquisition (431 CDSs), we speculated that the differences in antimicrobial susceptibility between the type strain and the isolates were largely influenced by the plasmids carried by the isolates.

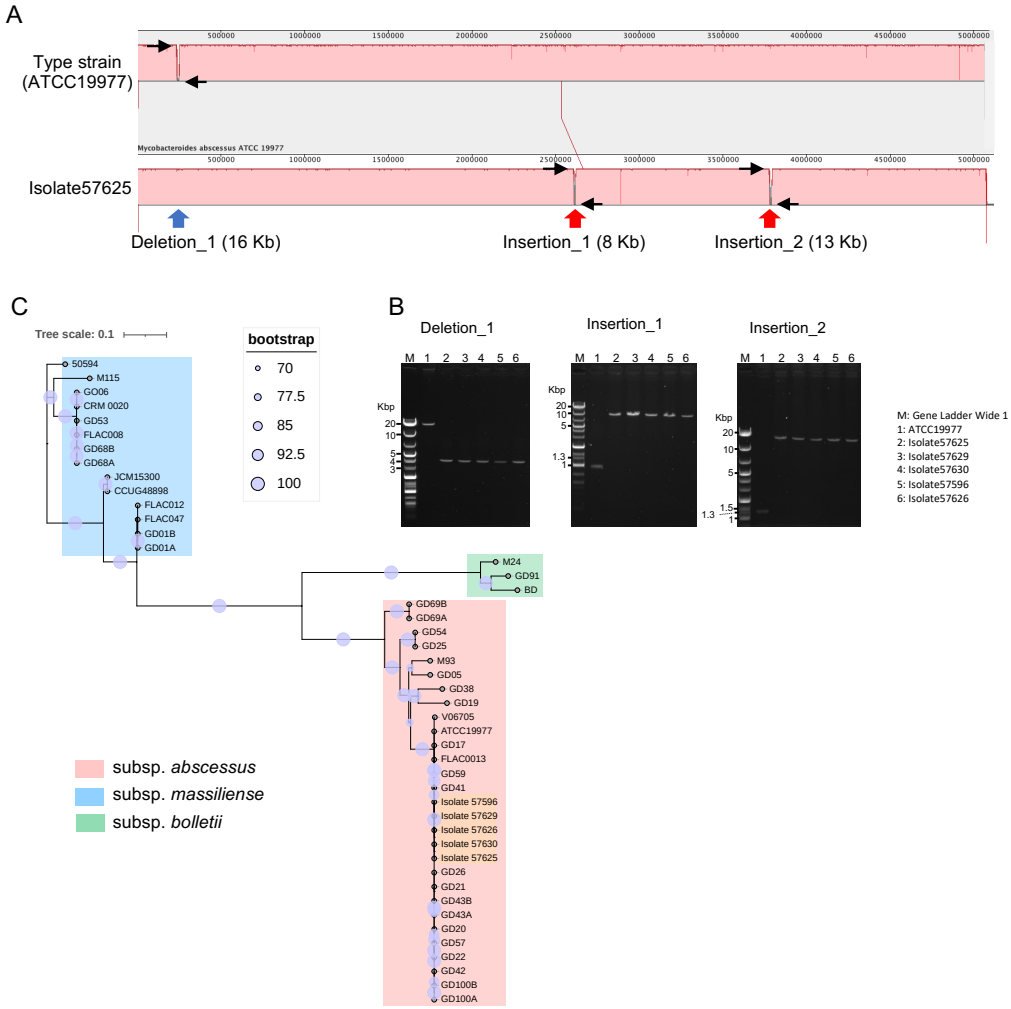

Figure 2. Comparison of the chromosome sequence of Isolate57625 with those of the type strain and other isolates. (**A**) The alignment of chromosome sequence of the type strain (ATCC 19977) and Isolate57625 detected three large structural variants (SVs). One deletion and two insertions were detected in the chromosome of the Isolate57625 compared to that of ATCC 19977. Black arrows indicated the primer region used for the validation of the SVs. (**B**) The validation of SVs using PCR. PCR was performed using the genomic DNA and the primers flanking the SVs. (**C**) The phylogenetic tree of the relevant isolates and other clinical isolates was constructed using the core SNVs detected in each chromosome sequence by the maximum likelihood method. Zero point one of the tree scale represents 10 % differences in the core SNVs. The bootstrap value (%) represents the probability that the same branch was observed when a phylogenetic tree was generated 1000 times.

Plasmid sequence analysis revealed that various virulence factors were encoded on the plasmids

Because the previous analysis suggested the involvement of plasmids in antimicrobial resistance to carbapenem in the isolates, we focused on the pMAB625 plasmids. It has been reported that the sequences of plasmids present in various bacteria have been deposited in the NCBI nucleotide database and can be searched using the PLSDB bacterial plasmid database (25). We then compared the plasmid sequences in the clinical isolates to known plasmid sequences using the PLSDB database and the MASH screening strategy (55). This analysis showed that pMAB625-3 and pMAB625-2 had homology with pGD69B-1 (accession number: NZ_CP065267) (identity, 99.9%; *p*-value, 0) and pGD21-2 (accession number: NZ_CP065286) (identity, 97.3%; *p*-value, 0), respectively (Figure 3A). Interestingly, pGD69B-1 and pGD21-2 were isolated from different clinical patients in the US in 2019, according to the information registered in Genbank. Given the genetic distance of the chromosomes between Isolate57625 and GD69B (the host of pGD69B-1) (Figure 2B), these two strains were considered to be different strains. Thus, at least pMAB625-3 appeared to be horizontally transferred between the different strains. On the other hand, because Isolate57625 and GD21 (the host of pGD21-2) were genetically close and could be identical strains, it was uncertain whether pMAB625-2 was transferred between these two strains. No plasmid homologous to pMAB625-1 was found by searching the PLSDB database.

Different plasmids may occasionally not be maintained simultaneously in individual bacteria due to plasmid incompatibility resuting from the replication mechanism or partitioning problem. Therefore, to verify the copy numbers of pMAB625 plasmids in the clinical isolates, we performed qPCR using primers specific for each plasmid. The plasmid copy number is shown as a relative value normalised using the copy number of *HrpA*, which is present in one copy on the chromosome. This analysis showed that the copy number of pMAB625-1 and pMAB625-2 was less than one per bacterium, and that of pMAB625-3 was more than five per bacterium in the isolates (Figure 3B). Therefore, the clinical isolates were considered to be a heterogeneous population in terms of plasmid possession.

We then investigated the function of the genes encoded on pMAB625 plasmids using homology searches. Plasmids encode various factors that influence host characteristics.

Therefore, to investigate the factors affecting antimicrobial susceptibility, we listed the lost and acquired genes in Isolate57625 compared to the type strain (Supplementary Table S4). Of note, 480 candidate ORFs were acquired and 37 candidate ORFs were lost in Isolate57625 compared to the type strain. We then searched the antimicrobial resistance genes from the various databases using Blast+ based on the amino acid sequences of the acquired candidate ORFs. This analysis showed that the CDS named Isolate57625_54550 had a similarity to *qacA*, a subunit of the qac multidrug efflux pump (56), (identity, 31 %; *e*-value, 1.69e-10; coverage, 16.1%) and that the CDS named Isolate57625_54800 had a similarity to *MexL*, a specific repressor of *MexJK* multidrug efflux system (57) (identity, 33%; *e*-value, 5.54e-4; coverage, 34.4%). However, the identity and coverage were not sufficiently high.

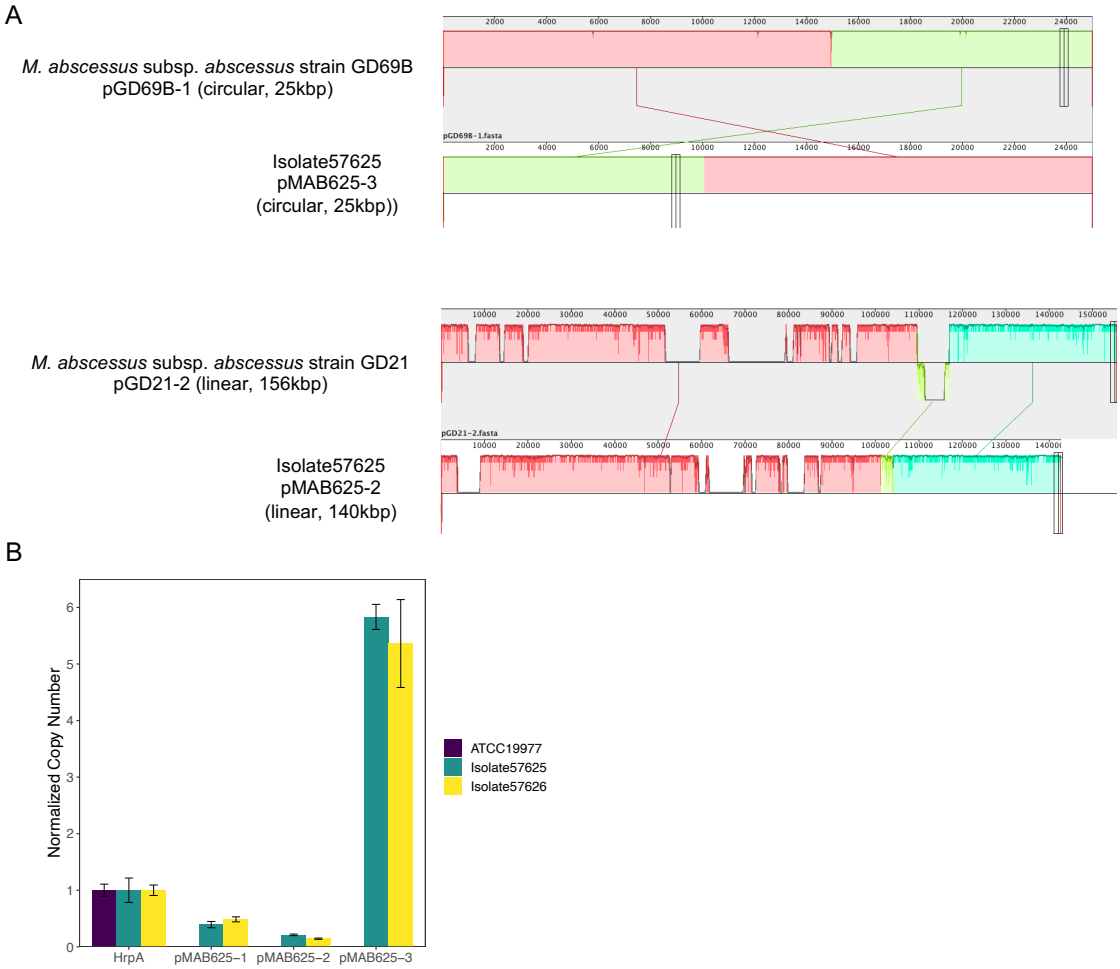

Figure 3. Homology search and copy number analysis of the plasmids that Isolate57625 harbour. (**A**) Plasmids that have homology with pMAB625 were searched using PLDBS (25). pMAB625-3 had homology with pGD69B-1 (identity: 99.9%) and pMAB625-2 did with pGD21-1 (identity: 97.3 %), however, pMAB625-1 did not have homology with any plasmids. (**B**) pMAB625 plasmid copy numbers in the type strain and each isolate were analysed by qPCR using primers specific to each plasmid. The normalised copy number represents the relative value that was normalized by the copy number of *HrpA* (encoded on the chromosome). The normalized copy number represents the mean of three independent experiments and the error bar represents the standard deviation.

To gain further insight into the effect of gene acquisition, we searched the homology of the acquired candidate ORFs using the mycobacterial gene database of Mycobrowser (44). This analysis detected 38 mycobacterial proteins with homology of amino acid to candidate

ORFs of the isolates. (identity > 30 %, *e*-value < 1e-50) (Supplementary Table S5). Notably, we found that genes associated with the ESX secretion system were highly enriched (10/38, 26%). ESX secretion systems are encoded in various bacteria on their chromosomes and plasmids. It has been reported that the ESX secretion system (also known as the type VII secretion system) is involved in bacterial virulence through several mechanisms, including evasion of the host immune system (58, 59), and biofilm formation (60). We further searched whether other ORFs of the components of the ESX secretion system were encoded near the loci of the detected ORFs of the components of the ESX secretion system using blast+. We detected several components of the ESX secretion system in pMAB625-1 and pMAB625-2 (Figure 4A). Core genes that construct membrane pores (*eccB, eccC, eccD, mycP,* and *eccE*) were present in these gene clusters. The type strain and clinical isolates have ESX-3 and ESX-4 loci on their chromosomes; therefore, the isolates acquired two additional ESX loci by the plasmid acquisition. To predict the function of these genes, we performed phylogenetic tree analysis using known amino acid sequences of the ESX secretion system components in chromosomes and plasmids. It was previously reported that plasmid-encoded ESX loci can be classified into 4 major clusters (61). Importantly, our analysis revealed that plasmid-encoded ESX loci were classified into 5 major clusters (ESX-P cluster 1-5) (Figure 4B). Notably, the newly classified ESX-P cluster 5 contained the ESX loci of pMAB625-1 and pMAB625-2. As shown in the plasmid sequence search results (Figure 3A), the ESX loci of pGD21-2 and pMAB625-2 were genetically related. Phylogenetic tree analysis also indicated that the ESX loci of pMAB625-1 were genetically close to those of pMFLV01, which was harboured by *Mycobacterium gilvum* PYR GCK. It was previously reported that pMFLV01 was enriched in biofilm formed in household water purifiers by metagenomic analysis (62). Biofilm formation is one of the drug resistance mechanisms in mycobacterium, and acts as a barrier against antibiotics. We also detected the toxin-antitoxin (TA) system components, YefM/YoeB and VapB5/VapC5 in pMAB625-1. The TA system is present in various bacteria and archaea and is encoded on their chromosomes and plasmids. It contributes to plasmid persistence, inhibiting bacteriophage propagation, and increases antimicrobial tolerance by inducing dormancy (63). These results indicated that the clinical isolates have acquired factors that could contribute to antimicrobial resistance through plasmid transfer.

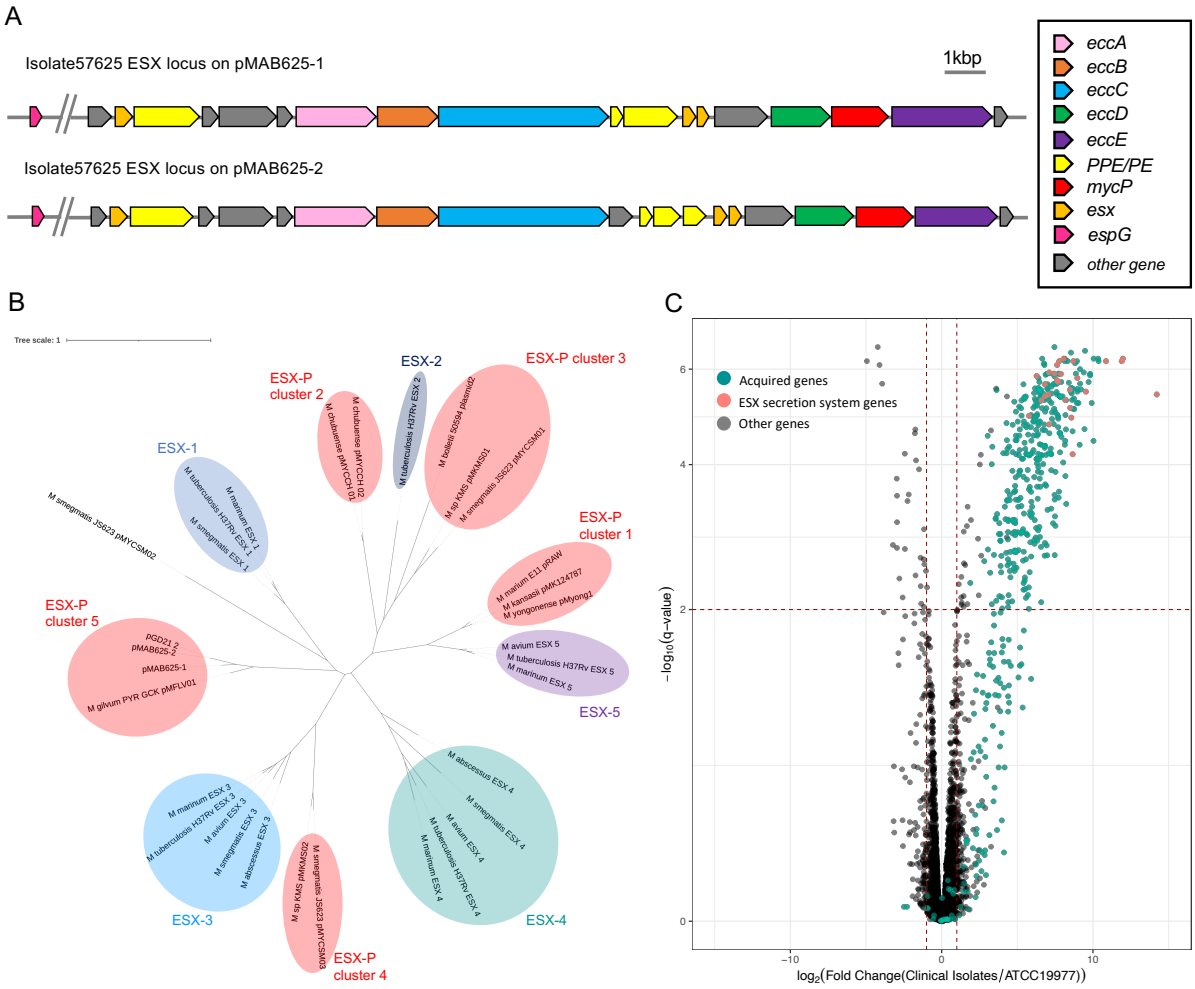

Figure 4. Phylogenetic and gene expression analysis of the genes related to the ESX secretion system. (**A**) The loci of the ESX secretion system are encoded on pMAB625-1 and pMAB625-2. CDS of the ESX secretion system were searched using Blast+. The core components that construct membrane pore (*eccB, eccC, eccD, mycP,* and *eccE*) are contained in this operon. (**B**) Phylogenetic tree analysis of various ESX loci encoded on chromosomes and plasmids. The amino acid sequence of the genes that construct the membrane pore were concatenated and the phylogenetic tree was created by NGphylogeny.fr (34) using the PhyML+SMS inference method. The classification of each cluster was followed as previously reported (61). (**C**) Volcano plot of RNA-seq analysis of the type strain and the isolates. The green dots represent the data of genes that the isolates acquired by SVs and plasmid acquisition. The red dots represent the data of ESX secretion system genes encoded on the plasmids. The dashed line on the X-axis represents the 2- and 0.5-fold change. The dashed line on the Y-axis represents the *q*-value of 0.01.

RNA-seq analysis

We found that the various genes associated with bacterial virulence were encoded on the pMAB625 plasmid. However, it was unclear whether genes encoded on these plasmids were expressed in the isolates and whether the gene expression from these plasmids affected the gene expression from the chromosome. To address these questions, we analysed the global gene expression in the type strain and the isolates using RNA-seq analysis (Figure 4C, Supplementary Table S6). In the clinical isolates, 393 genes were highly expressed and 29 genes were lowly expressed compared to the type strain. Although 25 genes and 29 genes carried by both the isolates and the type strains were highly and lowly expressed, 368 of the acquired genes were highly expressed and no acquired genes were lowly expressed in the isolates compared to the type strain. This result indicated that the transcription of genes on chromosomes was hardly affected by the transcription of genes on plasmids. Notably, the expression levels of the genes associated with the ESX secretion system, which were encoded on the pMAB625-1 and pMAB625-2, were 26- to 19016-fold higher in the isolates than in the type strain (Figure 4C). In addition, the genes associated with the TA system and the mycobacterial membrane protein large (MMPL) family transporter, which were also encoded on the pMAB625-1 and pMAB625-3, respectively, were highly expressed in the isolates compared to the type strain. These results indicated that the numerous genes associated with bacterial virulence encoded on the plasmids were more highly expressed in the clinical isolates than in the type strain, despite the low number of copies per bacterium regarding the pMAB625-1 and pMAB625-2.

Investigation of plasmid possession in the various clinical isolates worldwide

So far, we have found that the isolates carried three plasmids that the type strain did not, that these plasmids encoded the genes that could contribute to the antimicrobial resistance, and that these genes were also highly expressed in the isolates. However, we had analysed the strains sequentially isolated from only one patient and it was uncertain whether the plasmid acquisition occurred extensively in clinical isolates of mycobacterium. We therefore investigated whether other clinical isolates of mycobacterium carry the pMAB625 plasmids. We first performed PCR using the genomic DNA of the clinical isolates collected in Japan (14) with primers specific for each pMAB625 plasmid. We detected pMAB625-3 in two isolates

other than Isolate57625, although we did not detect pMAB625-1 and pMAB625-2 in any isolates other than Isolate57625 (Figure 5A). Both the isolates in which pMAB625-3 was detected were *M. abscessus*. We then verified the plasmid possession by mapping the read data from the short-read sequencer to the pMAB625 plasmid sequences. We used the read data of *M. abscessus* clinical isolates in Japan (48) obtained from the NCBI database in addition to our original data. Out of 125 clinical isolates, pMAB625-2 was detected in four isolates (3.2%) and pMAB625-3 was detected in 16 isolates (12.8%) (Table 3, Figure 5B). These isolates were collected from the four prefectures in Japan (Tokyo, Shizuoka, Aomori, and Okinawa) (Figure 5C). We confirmed that the read data of these isolates were mapped over the entire region of each plasmid. Although the coverage of the mapping data of DRR317396 was 37.4, it was only partially mapped and not counted. We also mapped the read data of the other mycobacterium species (three of *M. iranicum*, 20 of *M. fortuitum*, and 25 of *M. chelonae*), however, no pMAB625 plasmid was detected in these isolates (data not shown).

Moreover, to investigate whether clinical isolates in other areas of East Asia possess pMAB625 plasmids, we mapped the available read data about the clinical isolates from Taiwan and China. pMAB625-2 was detected in the isolates from China (2/69, 2.9%) and pMAB625-3 was detected in the isolates from Taiwan (7/98, 7.1%), and China (5/69, 7.2%) (Table 3, Supplementary Figure S3). Two plasmids were detected in ABS and MAS, but not in BOL.

Table 3. Summary of the possession of pMAB625 plasmids in the clinical isolates worldwide

	Number (%) of isolates*						
Region	Japan	China	Taiwan	Spain	UK	US	total
Analysed strains	125	69	98	30	30	110	462
with pMAB625-1	1 (0.8)	0	0	0	0	0	1 (0.2)
with pMAB625-2	4 (3.2)	2 (2.9)	0	0	2 (6.7)	2 (1.8)	10 (2.2)
with pMAB625-3	16 (12.8)	5 (7.2)	7 (7.1)	9 (30)	1 (3.3)	14 (12.7)	52 (11.3)

*The numbers outside parentheses represent the number of strains and the numbers in parentheses represent percentages.

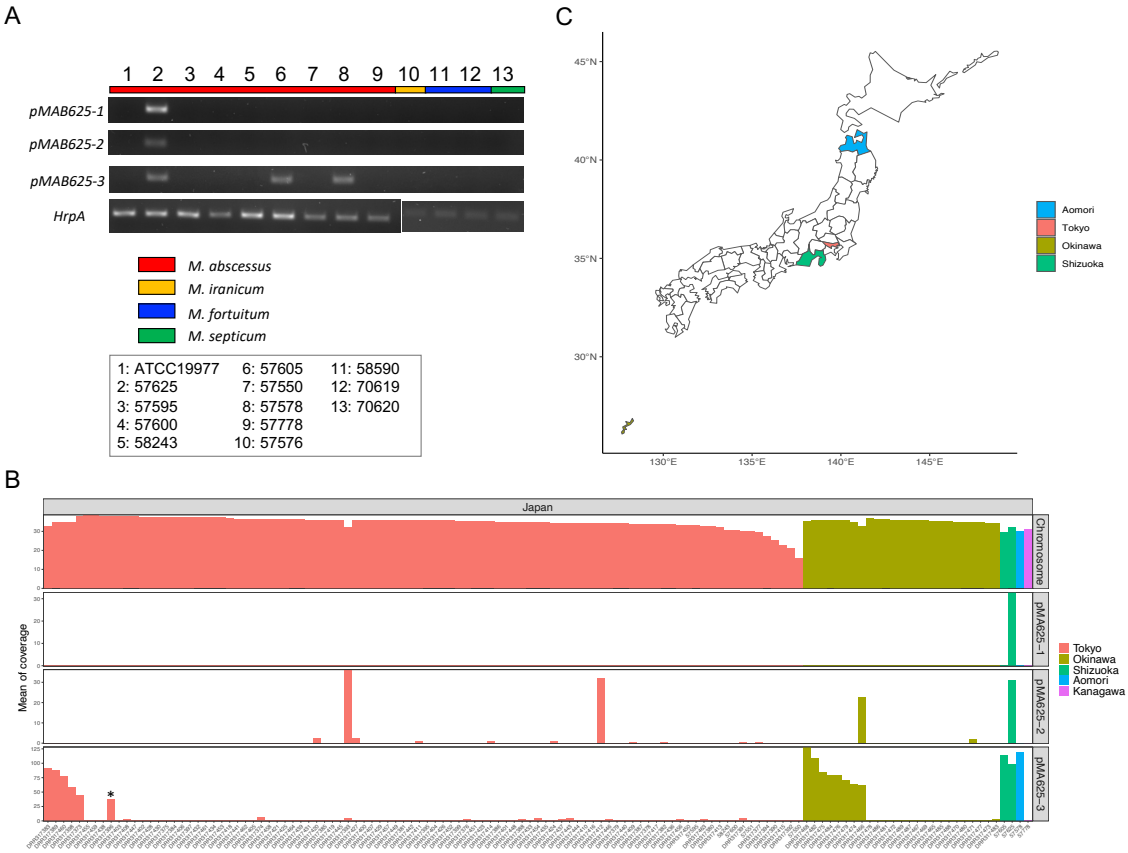

Figure 5. The possession of pMAB625 plasmid in the clinical isolates in Japan. (**A**) PCR analysis of the possession of pMAB625 plasmid in the clinical isolates which our group isolated in Japan. PCR was performed using the primers specific to each plasmid and *HrpA*. The colour bar represents the species of each isolate. The primer sets of *HrpA* were different depending on the species. (**B**) Mapping the read data of the clinical isolates in Japan to Isolate57625 genome sequence. The read data of the clinical isolates in Japan were downloaded from NCBI SRA and mapped using BWA-MEM to the sequence of Isolates57625. The mean of coverage to chromosome and each plasmid were plotted. The asterisk represents the strain whose coverage was high but whose read data was mapped only to the partial region of the plasmid. (**C**) Geographical map of Japan. The prefectures in which the pMAB625 plasmids were detected are represented by colour.

In addition, we analysed the clinical isolates in Spain, the UK, and the US to determine whether these isolates carried the pMAB625 plasmids (Figure 6). pMAB625-2 plasmid was detected in isolates from the UK (2/30, 6.7%), and the US (2/110, 1.8%). pMAB625-3 plasmid was detected in the isolates from Spain (9/30, 30%), the UK (1/30, 3.3%), and the US (14/110,

12.7%). Overall, pMAB625-1 was detected in one isolate (1/462, 0.2%), pMAB625-2 was detected in 10 isolates (10/462, 2.2%), and pMAB625-3 was detected in 52 isolates (52/462, 11.3%). These results indicated that pMAB625-2 and pMAB625-3 plasmids horizontally transferred between bacteria and subspecies in *M. abscessus* worldwide.

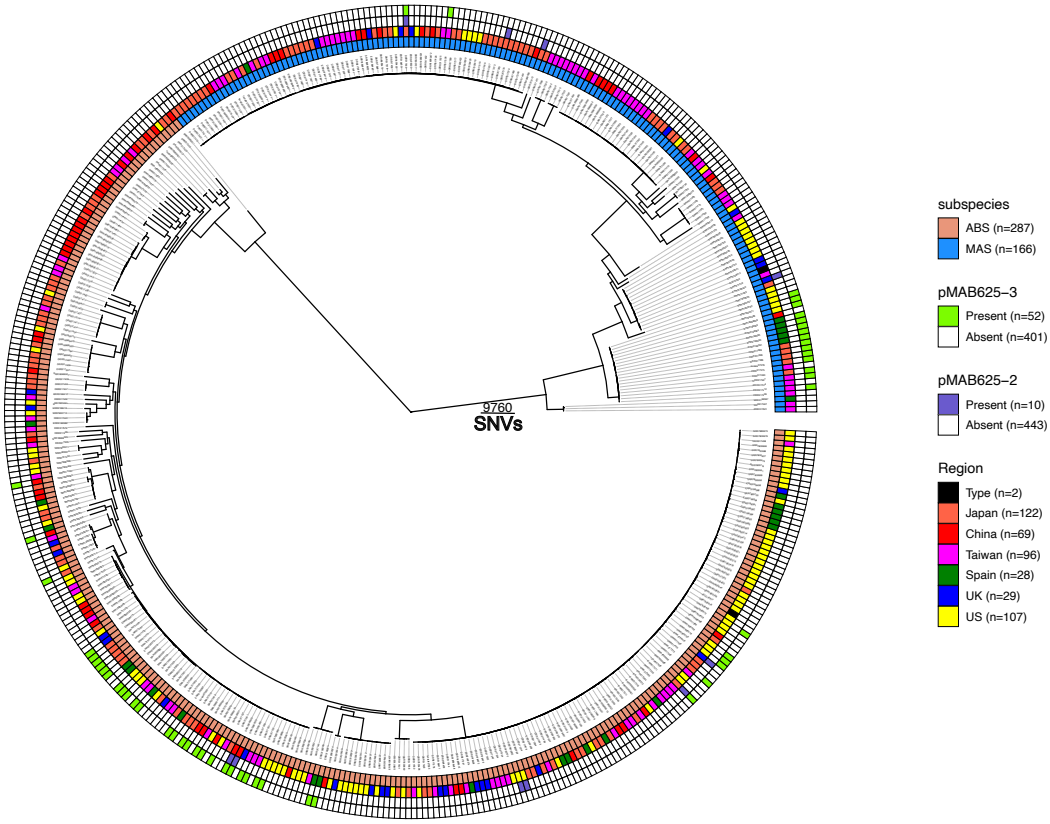

Figure 6. The possession of pMAB625 plasmid in clinical isolates worldwide. The read data of the clinical isolates collected worldwide were mapped to the pMAB625 plasmid sequences to verify the possession of the pMAB625 plasmids. The phylogenetic tree was created by Gubbins (53) using chromosome sequences and visualised by ggtree (54). Tree-scale represents the number of SNVs. The data of ABS and MAS but not BOL were used for the phylogenetic tree because no pMAB625 plasmid was detected in BOL.

To analyse the genetic relationship between plasmids, we compared the mapping results of clinical isolates to the pMAB625 plasmid and classified these sequences in terms of SVs and SNVs. The sequences of pMAB625-2 were classified into four types (Figure 7A). Assuming that Type I, which was the sequence of pMAB625-2 in Isolate57625, was the base sequence, Type II and III had the large SVs at Region B, and Type II but not Type III had at Region C. On the other hand, Type IV had large SVs at Region A and C, but not at Region B. Type I, Type III, and Type IV were detected in ABS, and Type II was detected in MAS, except for ERR3198514. In addition, Type III was detected only in the isolates collected in China, and Type IV was detected only in the isolates collected in the US. These results indicated that pMAB625-2 had been horizontally transferred between subspecies and had acquired the SVs unique to each subspecies and country.

There were no SNVs in the pMAB625-3 sequence of most isolates, however, there were SNVs in 13 out of 52 plasmid sequences (DRR317373, Japan; DRR317383, Japan; DRR317466, Japan; SRR18969469, China; SRR18969525, China; SRR7800511, US; SRR7800518, US; SRR7800703, US; SRR7800409, US; ERR3198385, Spain; ERR3198386, Spain; ERR3198395, Spain; ERR3198481, UK). Interestingly, in the six plasmid sequences (DRR317373, Japan; SRR18969469, China; SRR7800518, US; SRR7800703, US; SRR7800409, US; SRR7800511, US), the variant hotspot region was located at the CDS of the MMPL family transporter, which was the most reliably highly expressed gene in Isolate57625 and the other four isolates in the RNA-seq analysis. In addition, the variant pattern was classified into three types (Figure 7B). Four sequences (DRR317373, Japan; SRR7800518, US; SRR7800703, US; SRR7800409 US) were classified as Type A, and one sequence each was classified as Type B (SRR18969469, China) and Type C (SRR7800511, US). There were three missense mutations and 14 or 15 silent mutations in Type A, 20 missense mutations and 43 silent mutations in Type B, and 47 missense mutations and 126 silent mutations in Type C (Supplementary Table S7). Surprisingly, despite the large number of mutations, no mutation was responsible for the frameshift and nonsense mutations. It was therefore speculated that the mutant MMPL family transporters were being translated into full-length proteins in these isolates. These results suggested that the pMAB625 plasmid had acquired unique mutations in the process of transfer among bacteria across countries and subspecies around the world.

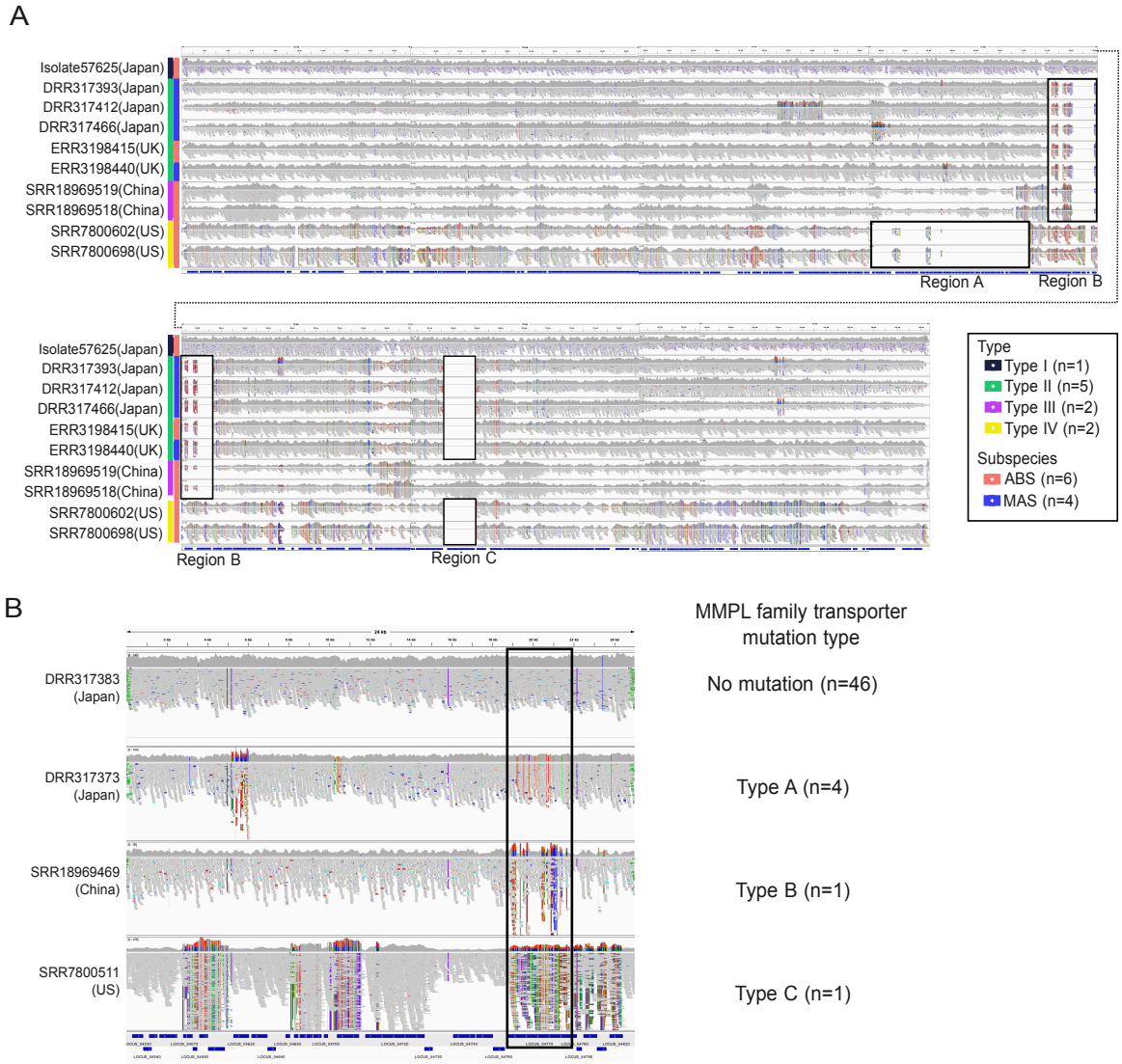

Figure 7. Comparison of the pMAB625-2 and pMAB625-3 sequences. (**A**) The mapping results of the reads data from each isolate to pMAB625-2 were visualised using IGV. Each sequence was classified into 4 types by the pattern of SNVs (surrounded by black line squares). (**B**) The mapping results of the reads data from each isolate to pMAB625-3 were also visualised by IGV. The mutation hotspot was located at the MMPL family transporter (surrounded by a black line square). The mutation types of the MMPL transporters were classified into three types and all mutations at this region were missense or silent mutations.

DISCUSSION

Plasmids are mobile genetic elements that can move between different bacterial strains and alter host characteristics, such as virulence, and antimicrobial susceptibility. However, it remains unclear whether plasmids confer antimicrobial resistance in *M. abscessus*. In this study, we showed that the multidrug-resistant clinical isolates of ABS isolated from a patient with osteomyelitis had chromosomes that were genetically close to the type strain and three plasmids (two of three were linear, and one was circular) that the type strain did not harbour. In addition, several factors associated with virulence and antimicrobial susceptibility were encoded on the plasmids, which were spread among clinical isolates around the world. To the best of our knowledge, this is the first report of common plasmid being spread in more than 10% of *M. abscessus* clinical isolates worldwide.

A recent study showed that prophages and plasmids in various clinical isolates contributed to diversity (64). They also reported that most strains have less than two types of plasmids and that strains with more than three types of plasmids were rare. Based on this report, Isolate57625 is a rare case. The copy number analysis indicated that Isolate57625 is a heterogeneous population with some remaining pMAB625-1 and pMAB625-2 but others not. Retaining plasmids is detrimental to bacterial growth, however, if genes for antimicrobial resistance are encoded on the plasmid, it is advantageous for survival during antimicrobial exposure. Therefore, a certain number of bacteria that retain the plasmid may be present in the population as a survival strategy against antimicrobial agents while growing as a population.

We identified various factors associated with multidrug resistance on the pMAB625 plasmids. The components of the ESX secretion system, the MMPL family transporter, and the components of the TA system were encoded on the plasmids, and these genes were highly expressed in the clinical isolates compared to the type strain. The ESX secretion system is involved in the export of the various pathogenic proteins and metal ions associated with proliferation, survival in the cytosol of macrophage, and conjugation. It has also been reported that ESX-1 components are required for sliding motility and biofilm formation in *M. avium* (60). Therefore, given the close genetic distance between ESX-1 and ESX-P cluster 5, which include the components of the ESX secretion system on the pMAB625-1 and pMAB625-2 (Figure 4B),

the components of ESX-P cluster 5 may be involved in biofilm formation. On the other hand, MMPL family transporters can transport antibiotics across the cell membrane. It has been reported that the increased expression of MMPL5 is associated with decreased susceptibility to bedaquiline, and clofazimine in *M. tuberculosis* (65, 66), bedaquiline, and clofazimine in *M. intracellulare* (67), and thiactazone derivative in *M. abscessus* (68). The function of the MMPL family transporter encoded on the pMAB625-3 is unknown; however, the presence of mutational hotspots indicates that this MMPL transporter may be compatible with a variety of substrates, including antimicrobial agents. Therefore, our results suggest that Isolate57625 enhanced defense mechanisms against antibiotics through the acquisition of the ESX secretion system and transporters, accompanied by changes in biofilm barriers, and transport of antibiotics. TA systems are known as the plasmid maintenance systems; however, they can transform the bacterial phenotype into dormancy by inhibiting vital cellular processes, such as proton-motive force and translation and contribute to antimicrobial torelance (69, 70). Thus, the acquisition of TA systems by the plasmid may be the cause of the decreased growth rate of Isolate57625 and Isolate57626 compared to the type strain (Figure 1). These results support that pMAB625 plasmids appeared to be the main cause of the low susceptibility to carbapenem antibiotics and intractability to treatment; however, further studies will be essential to determine whether these plasmids are the main cause of antimicrobial resistance.

As important findings, we found that 2.2% (10/462) and 11.3% (52/462) of the clinical isolates worldwide had pMAB625-2, and pMAB625-3, respectively. This result provides two significant insights. The first is an epidemiological insight into the spread of plasmids in *M. abscessus* beyond countries. Because *M. abscessus* has not been known to cause human-to-human transmission, this global spread of pMAB625 plasmids may be mainly due to increased global logistical activity and human mobility with associated interference of human and microbial habitats (71). The second is the potential of plasmids as pharmacological targets. The mechanisms of action of current antimicrobials inhibit specific cellular processes; therefore, protein mutation at the point of action or the acquisition of a multidrug transporter can lead to the emergence of resistant strains. Plasmids such as pMAB625-3, which are highly prevalent in multidrug-resistant bacteria, can be promising targets for the therapy using gene-editing methods such as CRISPR-Cas13a because these methods do not necessarily target genes or proteins that are targeted by conventional antibiotics. The CRISPR-Cas13a system can

recognise mRNA expressed not only from the loci on the chromosome but also on plasmids and induce non-specific RNA degradation and cell death (72). In addition, the gene-editing method can also target multiple regions of locus. Thus, the multiple, low-mutation loci encoded on plasmids, which are only found in antimicrobial-resistant bacteria, can be pharmaceutical targets that are robust to genetic mutations using the CRISPR-Cas13a system.

In summary, we have identified the plasmids that have been horizontally transferred among the multidrug-resistant *M. abscessus* clinical isolates worldwide. These findings provide a novel perspective on the acquisition of multidrug resistance in *M. abscessus*. Future studies will be required to verify whether the pMAB625 plasmids induce multidrug resistance in *M. abscessus* by plasmid transfection. These studies will lead to the development of robust therapies against multidrug resistance caused by genetic mutations, and a rapid daiagnostic method to prevent antibiotics abuse, and an understanding of the mechanisms of multidrug resistance in *M. abscessus*.

DATA AVAILABILITY

All raw sequence data and complete genome sequences generated in this study have been deposited in the DDBJ database with the BioProject accession number PRJDB16220.

SUPPLEMENTARY DATA

Supplementary Data are available at NAR online.

AUTHOR CONTRIBUTIONS

Kensuke Ohse: Conceptualization, Formal analysis, Methodology, Data curation, Investigation, Software, Validation, Visualization, Writing—original draft. Atushi Yoshida: Conceptualization, Methodology, Funding acquisition, Writing—original draft. Kamada Keisuke: Investigation. Hironobu Kitazawa, Yusuke Ito, Takayo Shoji, and Kenichiro Watanabe: Patient care and Resources. Hiroshi Koganemaru: Methodology, Patient care, and Resources. Ken Kikuchi: Investigation and Funding acquisition. Masashi Toyoda: Project administration, Supervision, Writing—review & editing.

ACKNOWLEDGEMENTS

The authors thank the staff of the microbiology laboratory of Dokkyo Medical University Hospital for performing identification and drug susceptibility tests, and Dr. Yoshishige Masuda and Dr. Takashi Inamatsu at TMIG for supervising in clinical practice. Computations were partially performed on the NIG supercomputer at ROIS National Institute of Genetics.

FUNDING

This work was supported by Japan Society for the Promotion of Science (JSPS) KAKENHI Grant Number JP19K08938.

CONFLICT OF INTEREST

None declared.

REFERENCES

1. Johansen,M.D., Herrmann,J.-L. and Kremer,L. (2020) Non-tuberculous mycobacteria and the rise of Mycobacterium abscessus. *Nat. Rev. Microbiol.*, **18**, 392–407.

2. Cristancho-Rojas,C., Varley,C.D., Lara,S.C., Kherabi,Y., Henkle,E. and Winthrop,K.L. (2024) Epidemiology of *Mycobacterium abscessus*. *Clin. Microbiol. Infect.*, **30**, 712–717.

3. Rubio,M., March,F., Garrigó,M., Moreno,C., Español,M. and Coll,P. (2015) Inducible and Acquired Clarithromycin Resistance in the Mycobacterium abscessus Complex. *PLoS ONE*, **10**, e0140166.

4. Huh,H.J., Kim,S.-Y., Jhun,B.W., Shin,S.J. and Koh,W.-J. (2019) Recent advances in molecular diagnostics and understanding mechanisms of drug resistance in nontuberculous mycobacterial diseases. *Infect. Genet. Evol.*, **72**, 169–182.

5. López-Roa,P., Esteban,J. and Muñoz-Egea,M.-C. (2023) Updated Review on the Mechanisms of Pathogenicity in Mycobacterium abscessus, a Rapidly Growing Emerging Pathogen. *Microorganisms*, **11**.

6. Clinical & Laboratory Standards Institute (2018) Susceptibility Testing of Mycobacteria, Nocardia spp., and Other Aerobic Actinomycetes, M24Ed3E.

7. Jong,B.-E., Wu,T.-S., Chen,N.-Y., Yang,C.-H., Shu,C.-C., Wang,L.-S., Wu,T.-L., Lu,J.-J., Chiu,C.-H., Lai,H.-C., *et al.* Impact on Macrolide Resistance of Genetic Diversity of Mycobacterium abscessus Species. *Microbiol. Spectr.*, **10**, e02749-22.

8. Solanki,P., Lipman,M., McHugh,T.D. and Satta,G. (2022) Whole genome sequencing and prediction of antimicrobial susceptibilities in non-tuberculous mycobacteria. *Front. Microbiol.*, **13**, 1044515.

9. Lipworth,S., Hough,N., Buchanan,R., Smith,E.G., Robinson,E., Alexander,E., Peto,T., Crook,D. and Walker,T. (2019) Improved Performance Predicting Clarithromycin Resistance in Mycobacterium abscessus on an Independent Data Set. *Antimicrob. Agents Chemother.*, **63**, e00400-19.

10. Akiyama,Y., Iwamoto,N., Kamada,K., Yoshida,A., Osugi,A., Mitarai,S., Suzuki,T., Yamamoto,K., Nagashima,M., Horai,T., *et al.* (2023) Aortic endograft infection by Mycobacterium abscessus subsp. massiliense with acquired clarithromycin resistance: a case report. *BMC Infect. Dis.*, **23**, 694.

11. Queenan,A.M. and Bush,K. (2007) Carbapenemases: the Versatile β-Lactamases. *Clin. Microbiol. Rev.*, **20**, 440–458.

12. Zhang,Y., Li,Z., He,X., Ding,F., Wu,W., Luo,Y., Fan,B. and Cao,H. (2017) Overproduction of efflux pumps caused reduced susceptibility to carbapenem under consecutive imipenem-selected stress in Acinetobacter baumannii. *Infect. Drug Resist.*, **11**, 457.

13. Ranjitkar,S., Reck,F., Ke,X., Zhu,Q., McEnroe,G., Lopez,S.L. and Dean,C.R. (2019) Identification of Mutations in the mrdA Gene Encoding PBP2 That Reduce Carbapenem and Diazabicyclooctane Susceptibility of Escherichia coli Clinical Isolates with Mutations in ftsI (PBP3) and Which Carry blaNDM-1. *mSphere*, **4**, e00074-19.

14. Kamada,K., Yoshida,A., Iguchi,S., Arai,Y., Uzawa,Y., Konno,S., Shimojima,M. and Kikuchi,K. (2021) Nationwide surveillance of antimicrobial susceptibility of 509 rapidly growing mycobacteria strains isolated from clinical specimens in Japan. *Sci. Rep.*, **11**, 12208.

15. Bouso,J.M. and Planet,P.J. (2019) Complete nontuberculous mycobacteria whole genomes using an optimized DNA extraction protocol for long-read sequencing. *BMC Genomics*, **20**, 793.

16. De Coster,W., D'Hert,S., Schultz,D.T., Cruts,M. and Van Broeckhoven,C. (2018) NanoPack: visualizing and processing long-read sequencing data. *Bioinformatics*, **34**, 2666–2669.

17. Wick,R.R., Judd,L.M., Gorrie,C.L. and Holt,K.E. (2017) Completing bacterial genome assemblies with multiplex MinION sequencing. *Microb. Genomics*, **3**, e000132.

18. Wang,J.R., Holt,J., McMillan,L. and Jones,C.D. (2018) FMLRC: Hybrid long read error correction using an FM-index. *BMC Bioinformatics*, **19**, 50.

19. Kolmogorov,M., Yuan,J., Lin,Y. and Pevzner,P.A. (2019) Assembly of long, error-prone reads using repeat graphs. *Nat. Biotechnol.*, **37**, 540–546.

20. Walker,B.J., Abeel,T., Shea,T., Priest,M., Abouelliel,A., Sakthikumar,S., Cuomo,C.A., Zeng,Q., Wortman,J., Young,S.K., *et al.* (2014) Pilon: An Integrated Tool for Comprehensive Microbial Variant Detection and Genome Assembly Improvement. *PLOS ONE*, **9**, e112963.

21. Gurevich,A., Saveliev,V., Vyahhi,N. and Tesler,G. (2013) QUAST: quality assessment tool for genome assemblies. *Bioinformatics*, **29**, 1072–1075.

22. Wick,R.R., Schultz,M.B., Zobel,J. and Holt,K.E. (2015) Bandage: interactive visualization of de novo genome assemblies. *Bioinformatics*, **31**, 3350–3352.

23. Tanizawa,Y., Fujisawa,T. and Nakamura,Y. (2018) DFAST: a flexible prokaryotic genome annotation pipeline for faster genome publication. *Bioinformatics*, **34**, 1037–1039.

24. Tanizawa,Y., Fujisawa,T., Kaminuma,E., Nakamura,Y. and Arita,M. (2016) DFAST and DAGA: web-based integrated genome annotation tools and resources. *Biosci. Microbiota Food Health*, **35**, 173–184.

25. Schmartz,G.P., Hartung,A., Hirsch,P., Kern,F., Fehlmann,T., Müller,R. and Keller,A. (2022) PLSDB: advancing a comprehensive database of bacterial plasmids. *Nucleic Acids Res.*, **50**, D273–D278.

26. Li,H. (2013) Aligning sequence reads, clone sequences and assembly contigs with BWA-MEM. 10.48550/arXiv.1303.3997.

27. Danecek,P., Bonfield,J.K., Liddle,J., Marshall,J., Ohan,V., Pollard,M.O., Whitwham,A., Keane,T., McCarthy,S.A., Davies,R.M., *et al.* (2021) Twelve years of SAMtools and BCFtools. *GigaScience*, **10**, giab008.

28. Garrison,E. and Marth,G. (2012) Haplotype-based variant detection from short-read sequencing. 10.48550/arXiv.1207.3907.

29. Cingolani,P., Platts,A., Wang,L.L., Coon,M., Nguyen,T., Wang,L., Land,S.J., Lu,X. and Ruden,D.M. (2012) A program for annotating and predicting the effects of single nucleotide polymorphisms, SnpEff: SNPs in the genome of Drosophila melanogaster strain w ^{1118}; iso-2; iso-3. *Fly (Austin)*, **6**, 80–92.

30. Darling,A.C.E., Mau,B., Blattner,F.R. and Perna,N.T. (2004) Mauve: Multiple Alignment of Conserved Genomic Sequence With Rearrangements. *Genome Res.*, **14**, 1394–1403.

31. Li,H. (2018) Minimap2: pairwise alignment for nucleotide sequences. *Bioinformatics*, **34**, 3094–3100.

32. Minh,B.Q., Schmidt,H.A., Chernomor,O., Schrempf,D., Woodhams,M.D., von Haeseler,A. and Lanfear,R. (2020) IQ-TREE 2: New Models and Efficient Methods for Phylogenetic Inference in the Genomic Era. *Mol. Biol. Evol.*, **37**, 1530–1534.

33. Letunic,I. and Bork,P. (2021) Interactive Tree Of Life (iTOL) v5: an online tool for phylogenetic tree display and annotation. *Nucleic Acids Res.*, **49**, W293–W296.

34. Lemoine,F., Correia,D., Lefort,V., Doppelt-Azeroual,O., Mareuil,F., Cohen-Boulakia,S. and Gascuel,O. (2019) NGPhylogeny.fr: new generation phylogenetic services for non-specialists. *Nucleic Acids Res.*, **47**, W260–W265.

35. Camacho,C., Coulouris,G., Avagyan,V., Ma,N., Papadopoulos,J., Bealer,K. and Madden,T.L. (2009) BLAST+: architecture and applications. *BMC Bioinformatics*, **10**, 421.

36. Feldgarden,M., Brover,V., Haft,D.H., Prasad,A.B., Slotta,D.J., Tolstoy,I., Tyson,G.H., Zhao,S., Hsu,C.-H., McDermott,P.F., *et al.* (2019) Validating the AMRFinder Tool and Resistance Gene Database by Using Antimicrobial Resistance Genotype-Phenotype Correlations in a Collection of Isolates. *Antimicrob. Agents Chemother.*, **63**, e00483-19.

37. Jia,B., Raphenya,A.R., Alcock,B., Waglechner,N., Guo,P., Tsang,K.K., Lago,B.A., Dave,B.M., Pereira,S., Sharma,A.N., *et al.* (2017) CARD 2017: expansion and model-

centric curation of the comprehensive antibiotic resistance database. *Nucleic Acids Res.*, **45**, D566–D573.

38. Zankari,E., Hasman,H., Cosentino,S., Vestergaard,M., Rasmussen,S., Lund,O., Aarestrup,F.M. and Larsen,M.V. (2012) Identification of acquired antimicrobial resistance genes. *J. Antimicrob. Chemother.*, **67**, 2640–2644.

39. Gupta,S.K., Padmanabhan,B.R., Diene,S.M., Lopez-Rojas,R., Kempf,M., Landraud,L. and Rolain,J.-M. (2014) ARG-ANNOT, a New Bioinformatic Tool To Discover Antibiotic Resistance Genes in Bacterial Genomes. *Antimicrob. Agents Chemother.*, **58**, 212–220.

40. Chen,L., Zheng,D., Liu,B., Yang,J. and Jin,Q. (2016) VFDB 2016: hierarchical and refined dataset for big data analysis—10 years on. *Nucleic Acids Res.*, **44**, D694–D697.

41. Carattoli,A., Zankari,E., García-Fernández,A., Voldby Larsen,M., Lund,O., Villa,L., Møller Aarestrup,F. and Hasman,H. (2014) In Silico Detection and Typing of Plasmids using PlasmidFinder and Plasmid Multilocus Sequence Typing. *Antimicrob. Agents Chemother.*, **58**, 3895–3903.

42. Ingle,D.J., Valcanis,M., Kuzevski,A., Tauschek,M., Inouye,M., Stinear,T., Levine,M.M., Robins-Browne,R.M. and Holt,K.E. (2016) In silico serotyping of E. coli from short read data identifies limited novel O-loci but extensive diversity of O:H serotype combinations within and between pathogenic lineages. *Microb. Genomics*, **2**, e000064.

43. Doster,E., Lakin,S.M., Dean,C.J., Wolfe,C., Young,J.G., Boucher,C., Belk,K.E., Noyes,N.R. and Morley,P.S. (2020) MEGARes 2.0: a database for classification of antimicrobial drug, biocide and metal resistance determinants in metagenomic sequence data. *Nucleic Acids Res.*, **48**, D561–D569.

44. Kapopoulou,A., Lew,J.M. and Cole,S.T. (2011) The MycoBrowser portal: a comprehensive and manually annotated resource for mycobacterial genomes. *Tuberc. Edinb. Scotl.*, **91**, 8–13.

45. Kim,D., Langmead,B. and Salzberg,S.L. (2015) HISAT: a fast spliced aligner with low memory requirements. *Nat. Methods*, **12**, 357–360.

46. Pertea,M., Pertea,G.M., Antonescu,C.M., Chang,T.-C., Mendell,J.T. and Salzberg,S.L. (2015) StringTie enables improved reconstruction of a transcriptome from RNA-seq reads. *Nat. Biotechnol.*, **33**, 290–295.

47. Sun,J., Nishiyama,T., Shimizu,K. and Kadota,K. (2013) TCC: an R package for comparing tag count data with robust normalization strategies. *BMC Bioinformatics*, **14**, 219.

48. Yoshida,M., Chien,J.-Y., Morimoto,K., Kinjo,T., Aono,A., Murase,Y., Fujiwara,K., Morishige,Y., Nagano,H., Jou,R., *et al.* (2022) Molecular Epidemiological Characteristics of Mycobacterium abscessus Complex Derived from Non-Cystic Fibrosis Patients in Japan and Taiwan. *Microbiol. Spectr.*, **10**, e00571-22.

49. Jin,P., Dai,J., Guo,Y., Wang,X., Lu,J., Zhu,Y. and Yu,F. (2022) Genomic Analysis of Mycobacterium abscessus Complex Isolates from Patients with Pulmonary Infection in China. *Microbiol. Spectr.*, **10**, e00118-22.

50. Chen,S. (2023) Ultrafast one-pass FASTQ data preprocessing, quality control, and deduplication using fastp. *iMeta*, **2**, e107.

51. Shen,W., Le,S., Li,Y. and Hu,F. (2016) SeqKit: A Cross-Platform and Ultrafast Toolkit for FASTA/Q File Manipulation. *PLOS ONE*, **11**, e0163962.

52. García-Alcalde,F., Okonechnikov,K., Carbonell,J., Cruz,L.M., Götz,S., Tarazona,S., Dopazo,J., Meyer,T.F. and Conesa,A. (2012) Qualimap: evaluating next-generation sequencing alignment data. *Bioinformatics*, **28**, 2678–2679.

53. Croucher,N.J., Page,A.J., Connor,T.R., Delaney,A.J., Keane,J.A., Bentley,S.D., Parkhill,J. and Harris,S.R. (2015) Rapid phylogenetic analysis of large samples of recombinant bacterial whole genome sequences using Gubbins. *Nucleic Acids Res.*, **43**, e15.

54. Yu,G., Smith,D.K., Zhu,H., Guan,Y. and Lam,T.T.-Y. (2017) ggtree: an r package for visualization and annotation of phylogenetic trees with their covariates and other associated data. *Methods Ecol. Evol.*, **8**, 28–36.

55. Ondov,B.D., Starrett,G.J., Sappington,A., Kostic,A., Koren,S., Buck,C.B. and Phillippy,A.M. (2019) Mash Screen: high-throughput sequence containment estimation for genome discovery. *Genome Biol.*, **20**, 232.

56. Paulsen,I.T., Brown,M.H., Littlejohn,T.G., Mitchell,B.A. and Skurray,R.A. (1996) Multidrug resistance proteins QacA and QacB from Staphylococcus aureus: membrane topology and identification of residues involved in substrate specificity. *Proc. Natl. Acad. Sci.*, **93**, 3630–3635.

57. Chuanchuen,R., Gaynor,J.B., Karkhoff-Schweizer,R. and Schweizer,H.P. (2005) Molecular Characterization of MexL, the Transcriptional Repressor of the mexJK Multidrug Efflux Operon in Pseudomonas aeruginosa. *Antimicrob. Agents Chemother.*, **49**, 1844–1851.

58. Osman,M.M., Shanahan,J.K., Chu,F., Takaki,K.K., Pinckert,M.L., Pagán,A.J., Brosch,R., Conrad,W.H. and Ramakrishnan,L. (2022) The C terminus of the mycobacterium ESX-1 secretion system substrate ESAT-6 is required for phagosomal membrane damage and virulence. *Proc. Natl. Acad. Sci.*, **119**, e2122161119.

59. Laencina,L., Dubois,V., Le Moigne,V., Viljoen,A., Majlessi,L., Pritchard,J., Bernut,A., Piel,L., Roux,A.-L., Gaillard,J.-L., *et al.* (2018) Identification of genes required for Mycobacterium abscessus growth in vivo with a prominent role of the ESX-4 locus. *Proc. Natl. Acad. Sci.*, **115**, E1002–E1011.

60. Lai,L.-Y., Lin,T.-L., Chen,Y.-Y., Hsieh,P.-F. and Wang,J.-T. (2018) Role of the Mycobacterium marinum ESX-1 Secretion System in Sliding Motility and Biofilm Formation. *Front. Microbiol.*, **9**, 1160.

61. Dumas,E., Christina Boritsch,E., Vandenbogaert,M., Rodríguez de la Vega,R.C., Thiberge,J.-M., Caro,V., Gaillard,J.-L., Heym,B., Girard-Misguich,F., Brosch,R., *et al.* (2016) Mycobacterial Pan-Genome Analysis Suggests Important Role of Plasmids in the Radiation of Type VII Secretion Systems. *Genome Biol. Evol.*, **8**, 387–402.

62. Zhou,Z., Xu,L., Zhu,L., Liu,Y., Shuai,X., Lin,Z. and Chen,H. (2021) Metagenomic analysis of microbiota and antibiotic resistome in household activated carbon drinking water purifiers. *Environ. Int.*, **148**, 106394.

63. Harms,A., Brodersen,D.E., Mitarai,N. and Gerdes,K. (2018) Toxins, Targets, and Triggers: An Overview of Toxin-Antitoxin Biology. *Mol. Cell*, **70**, 768–784.

64. Dedrick,R.M., Aull,H.G., Jacobs-Sera,D., Garlena,R.A., Russell,D.A., Smith,B.E., Mahalingam,V., Abad,L., Gauthier,C.H. and Hatfull,G.F. (2021) The Prophage and Plasmid Mobilome as a Likely Driver of Mycobacterium abscessus Diversity. *mBio*, **12**, e03441-20.

65. Andries,K., Villellas,C., Coeck,N., Thys,K., Gevers,T., Vranckx,L., Lounis,N., Jong,B.C. de and Koul,A. (2014) Acquired Resistance of Mycobacterium tuberculosis to Bedaquiline. *PLOS ONE*, **9**, e102135.

66. Hartkoorn,R.C., Uplekar,S. and Cole,S.T. (2014) Cross-Resistance between Clofazimine and Bedaquiline through Upregulation of MmpL5 in Mycobacterium tuberculosis. *Antimicrob. Agents Chemother.*, **58**, 2979–2981.

67. Alexander,D.C., Vasireddy,R., Vasireddy,S., Philley,J.V., Brown-Elliott,B.A., Perry,B.J., Griffith,D.E., Benwill,J.L., Cameron,A.D.S. and Wallace,R.J. (2017) Emergence of mmpT5 Variants during Bedaquiline Treatment of Mycobacterium intracellulare Lung Disease. *J. Clin. Microbiol.*, **55**, 574–584.

68. Halloum,I., Viljoen,A., Khanna,V., Craig,D., Bouchier,C., Brosch,R., Coxon,G. and Kremer,L. (2017) Resistance to Thiacetazone Derivatives Active against Mycobacterium abscessus Involves Mutations in the MmpL5 Transcriptional Repressor MAB_4384. *Antimicrob. Agents Chemother.*, **61**, e02509-16.

69. Sonika,S., Singh,S., Mishra,S. and Verma,S. (2023) Toxin-antitoxin systems in bacterial pathogenesis. *Heliyon*, **9**, e14220.

70. Harms,A., Maisonneuve,E. and Gerdes,K. (2016) Mechanisms of bacterial persistence during stress and antibiotic exposure. *Science*, **354**, aaf4268.

71. Castañeda-Barba,S., Top,E.M. and Stalder,T. (2024) Plasmids, a molecular cornerstone of antimicrobial resistance in the One Health era. *Nat. Rev. Microbiol.*, **22**, 18–32.

72. Kiga,K., Tan,X.-E., Ibarra-Chávez,R., Watanabe,S., Aiba,Y., Sato'o,Y., Li,F.-Y., Sasahara,T., Cui,B., Kawauchi,M., *et al.* (2020) Development of CRISPR-Cas13a-based antimicrobials capable of sequence-specific killing of target bacteria. *Nat. Commun.*, **11**, 2934.

TABLE AND FIGURES LEGENDS

Figure 1. Growth curve of the type strain and the isolates. The type strain (ATCC 19977) and the isolates were inoculated with the same seeding concentration and cultivated at 30 °C. OD_{600} was measured at each time point. Data represents the mean of the three independent experiments and the error bar represents the standard deviation. Asterisks represent the statistical significance between ATCC 19977 and each isolate. *p*-value were calculated using one-way ANOVA followed by Dunnett's test (**p*<0.01, ***p*<0.001).

Figure 2. Comparison of the chromosome sequence of Isolate57625 with those of the type strain and other isolates. (**A**) The alignment of chromosome sequence of the type strain (ATCC 19977) and Isolate57625 detected three large structural variants (SVs). One deletion and two insertions were detected in the chromosome of the Isolate57625 compared to that of ATCC 19977. Black arrows indicated the primer region used for the validation of the SVs. (**B**) The validation of SVs using PCR. PCR was performed using the genomic DNA and the primers flanking the SVs. (**C**) The phylogenetic tree of the relevant isolates and other clinical isolates was constructed using the core SNVs detected in each chromosome sequence by the maximum likelihood method. Zero point one of the tree scale represents 10 % differences in the core SNVs. The bootstrap value (%) represents the probability that the same branch was observed when a phylogenetic tree was generated 1000 times.

Figure 3. Homology search and copy number analysis of the plasmids that Isolate57625 harbour. (**A**) Plasmids that have homology with pMAB625 were searched using PLDBS (25). pMAB625-3 had homology with pGD69B-1 (identity: 99.9%) and pMAB625-2 did with pGD21-1 (identity: 97.3 %), however, pMAB625-1 did not have homology with any plasmids. (**B**) pMAB625 plasmid copy numbers in the type strain and each isolate were analysed by qPCR using primers specific to each plasmid. The normalised copy number represents the relative value that was normalized by the copy number of *HrpA* (encoded on the chromosome). The normalized copy number represents the mean of three independent experiments and the error bar represents the standard deviation.

Figure 4. Phylogenetic and gene expression analysis of the genes related to the ESX secretion system. (**A**) The loci of the ESX secretion system are encoded on pMAB625-1 and pMAB625-2. CDS of the ESX secretion system were searched using Blast+. The core components that construct membrane pore (*eccB, eccC, eccD, mycP,* and *eccE*) are contained in this operon. (**B**) Phylogenetic tree analysis of various ESX loci encoded on chromosomes and plasmids. The amino acid sequence of the genes that construct the membrane pore were concatenated and

the phylogenetic tree was created by NGphylogeny.fr (34) using the PhyML+SMS inference method. The classification of each cluster was followed as previously reported (61). (**C**) Volcano plot of RNA-seq analysis of the type strain and the isolates. The green dots represent the data of genes that the isolates acquired by SVs and plasmid acquisition. The red dots represent the data of ESX secretion system genes encoded on the plasmids. The dashed line on the X-axis represents the 2- and 0.5-fold change. The dashed line on the Y-axis represents the *q*-value of 0.01.

Figure 5. The possession of pMAB625 plasmid in the clinical isolates in Japan. (**A**) PCR analysis of the possession of pMAB625 plasmid in the clinical isolates which our group isolated in Japan. PCR was performed using the primers specific to each plasmid and *HrpA*. The colour bar represents the species of each isolate. The primer sets of *HrpA* were different depending on the species. (**B**) Mapping the read data of the clinical isolates in Japan to Isolate57625 genome sequence. The read data of the clinical isolates in Japan were downloaded from NCBI SRA and mapped using BWA-MEM to the sequence of Isolates57625. The mean of coverage to chromosome and each plasmid were plotted. The asterisk represents the strain whose coverage was high but whose read data was mapped only to the partial region of the plasmid. (**C**) Geographical map of Japan. The prefectures in which the pMAB625 plasmids were detected are represented by colour.

Figure 6. The possession of pMAB625 plasmid in clinical isolates worldwide. The read data of the clinical isolates collected worldwide were mapped to the pMAB625 plasmid sequences to verify the possession of the pMAB625 plasmids. The phylogenetic tree was created by Gubbins (53) using chromosome sequences and visualised by ggtree (54). Tree-scale represents the number of SNVs. The data of ABS and MAS but not BOL were used for the phylogenetic tree because no pMAB625 plasmid was detected in BOL.

Figure 7. Comparison of the pMAB625-2 and pMAB625-3 sequences. (**A**) The mapping results of the reads data from each isolate to pMAB625-2 were visualised using IGV. Each

sequence was classified into 4 types by the pattern of SNVs (surrounded by black line squares). (**B**) The mapping results of the reads data from each isolate to pMAB625-3 were also visualised by IGV. The mutation hotspot was located at the MMPL family transporter (surrounded by a black line square). The mutation types of the MMPL transporters were classified into three types and all mutations at this region were missense or silent mutations.

Table 1. The isolation time point of the clinical isolates and antimicrobial susceptibility of the type strain and the isolates. *MICs were determined as the minimum concentration at which the bacteria did not grow. No antimicrobial susceptibility testing was conducted on the isolates other than Isolate57625 and Isolate57626, representing hyphens in the table. The test was repeated three times and all MICs were confirmed to be the same between the experiments with exception of imipenem for the isolates. AMK, Amikacin; TOB, Tobramycin; IPM, Imipenem; FRPM, Faropenem; LVFX, Levofloxacin; MFLX, Moxifloxacin; AZM, Azithromycin; CAM, Clarithromycin; ST, Trimethoprim/sulfamethoxazole; DOXY, Doxycycline; MEPM, Meropenem; LNZ, Linezolid; CLF, Clofazimine; STFX, Sitafloxacin

†For Isolate57625, the MICs against IPM in the three experiments were 64, 16, and 16 μg/mL, respectively.

‡For Isolate57626, the MICs against IPM in the three experimenst were >64, 16, and >64 μg/mL, respectively.

Table 2. Genome assembly and the annotation statics of the Isolate57625.

Table 3. Summary of the possession of pMAB625 plasmids in the clinical isolates worldwide. *The numbers outside parentheses represent the number of strains and the numbers in parentheses represent percentages.